Chapter 1

A Guide to Fiber Bragg Grating Sensors

Marcelo M. Werneck, Regina C. S. B. Allil, Bessie A. Ribeiro and Fábio V. B. de Nazaré

Additional information is available at the end of the chapter

http://dx.doi.org/10.5772/54682

1. Introduction

Optical fiber sensors (OFS) appeared just after the invention of the practical optical fiber by Corning Glass Works in 1970, now Corning Incorporated, that produced the first fiber with losses below 20 dB/km. At the beginning of this era, optical devices such as laser, photodetectors and the optical fibers were very expensive, afforded only by telecom companies to circumvent the old saturated copper telephone network. With the great diffusion of the optical fiber technology during the 1980's and on, optoelectronic devices became less expensive, what favored their use in OFS.

OFS can be applied in many branches of the industry but we will concentrate here the electrical power industry. In this area, the operators need to measure and monitor some important physical parameters that include:

- Strain ($\mu\epsilon$)
- Vibration of structures and machines
- Electric current (from A to kA)
- Voltage (from mV to MV)
- Impedance ($\mu\Omega$)
- Leakage current of insulators (μA to mA)
- Temperature
- Pressure
- Gas concentration
- Distance between stationary and rotating or moving parts

In the electrical power industry (EPI) we have two facts that can cause collapse of an electronic sensor: presence of high voltage and presence of high electromagnetic interference. Therefore, depending on where we want to measure a parameter it can be very difficult or even impossible to use a conventional sensor. The best option to circumvent this

is through the use of an OFS, because the fiber is made of dielectric material sand, therefore, it is possible to place them very close or even over a high potential conductor and they do not necessarily need electrical power at the sensor location.

Another problem with conventional sensors is that they all need electric energy to work. However, providing electric energy at the sensor location is sometimes difficult if the device needs to be far away from any appropriated power supply. It happens in long high voltage transmission lines, at high voltage potentials, along pipe-lines or in deep ocean, for instance. Since OFS are passive sensors they do not need electric energy to work.

Therefore we can mention some, very specific characteristics of OFS that are well exploited when applied to the EPI:

- High immunity to Electromagnetic Interference (EMI)
- Electrical insulation
- Absence of metallic parts
- Local electrical power not required
- Lightweight and compactness
- Easy maintenance
- Chemically inert even against corrosion
- Work over long distances
- Several sensors can be multiplexed on the same fiber

There are many options to develop an OFS. The easiest way is by making the measurement to modulate the light amplitude that is the power, and ending up with an amplitude modulated sensor. These sensors were very common at the beginning of OFS era but they gradually were substituted by wavelength based sensors. These are more stable and self-calibrated as the wavelength does not depend on losses due connectors, modal drifts, macro bends, or LED and LASER ageing/drifts.

In this Chapter we will concentrate on a very special type of OFS: the Fiber Bragg Grating (FBG) sensors.

2. Theory and models of FBG

Fiber Bragg Grating (FBG) technology is one of the most popular choices for optical fiber sensors for strain or temperature measurements due to their simple manufacture, as we will see later on, and due to the relatively strong reflected signal. They are formed by a periodic modulations of the index of refraction of the fiber core along the longitudinal direction and can be produced by various techniques. The term fiber Bragg grating was borrowed from the Bragg law and applied to the periodical structures inscribed inside the core of conventional telecom fiber. Therefore, before entering the theory of fiber Bragg grating itself, it is worth to go back one century behind in order to review the Bragg law.

Sir William Lawrence Bragg, was born in 1890, a British physicist and X-ray crystallographer, was the discoverer, in 1912, of the Bragg law of X-ray diffraction. This

principle is used until today for the study and determination of crystal structure, particularly in thin film research. Sir Bragg, together with his father, won the Nobel Prize for Physics in 1915 for an important step in the development of X-ray crystallography.

Bragg diffraction occurs for an electromagnetic radiation whose wavelength is the same order of magnitude of the atomic spacing, when incident upon a crystalline material. In this case the radiation is scattered in a specular fashion by the atoms of the material and experiences constructive interference in accordance to Bragg's law. For a crystalline solid with lattice planes separated by a distance d the waves are scattered and interfere constructively if the path length of each wave is equal to an integer multiple of the wavelength. Figure 1 shows the idea. Bragg's law describes the condition for constructive interference from several crystallographic planes of the crystalline lattice separated by a distance d:

$$2d \sin\theta = n\lambda \tag{1}$$

Where θ is the incident angle, n is an integer and λ is the wavelength. A diffraction pattern is obtained by measuring the intensity of the scattered radiation as a function of the angle θ. Whenever the scattered waves satisfy the Bragg condition it is observed a strong intensity in the diffraction pattern, known as Bragg peak.

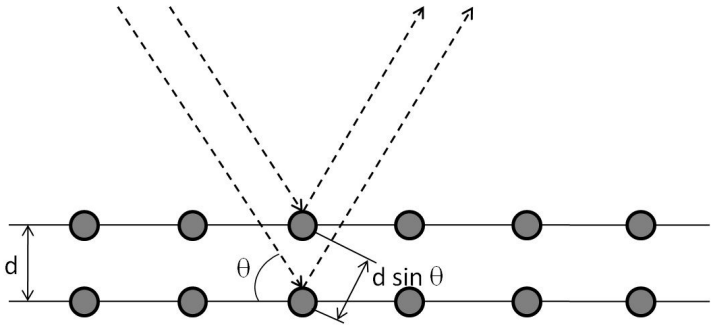

Figure 1. An incident radiation is reflected by the lattice structure of a crystal and will interfere constructively if the Bragg law is obeyed.

The first observations of index of refraction changes were noticed in germane silicate fibers and were reported by Kenneth Hill and co-workers in 1978 [1]. They described a permanent grating written in the core of the fiber by an argon ion laser line at 488 nm launched into the fiber by a microscope objective. This particular grating had a very weak index modulation, resulting in a narrow-band reflection filter at the writing wavelength. In reality, this phenomenon happened by chance, when they injected a high power blue light into de fiber, unexpectedly, after a few minutes, the transmitted light decayed. It was Friday but they were so puzzled with this phenomenon that Hill returned to his laboratory on Saturday to make a new experiment. He wanted to know where the light was going to and he had a clue. He used a thin microscope slide as a beam splitter in order to monitor a possible

reflection from the fiber and there was the missing light [2]. The explanation is that at the end of the fiber about 4% of the light was reflected by Fresnel reflection which, in its way backwards, interfered with the ongoing light producing an interference pattern. This pattern contained peaks and valleys of a stationary wave which imprinted permanently the pattern into the core of the fiber as an index of refraction modulation. Initially, the reflected light intensity is low, but after some time, it grows in intensity until almost all the light launched into the fiber is back-reflected. The growth in back-reflected light was explained in terms of a new effect called "photosensitivity".

After the inscription of the grating into de fiber's core, due the periodic modulation of the index of refraction, light guided along the core of the fiber will be weakly reflected by each grating plane by Fresnel effect. The reflected light from each grating plane will join together with the other reflections in the backward direction. This addition may be constructive or destructive, depending whether the wavelength of the incoming light meets the Bragg condition of Eq. (1).

Now, according to Eq. (1), since $\theta=90°$ and d is the distance between peaks of the interference pattern, $\lambda=2d$ for $n=1$ is the approximate wavelength of the reflection peak. That is, the fiber now acts as a dichroic mirror, reflecting part of the incoming spectrum. Equation (1), developed for vacuum, has to be adapted for silica, since the distances traveled by light are affected by the index of refraction of the fiber:

$$\lambda_B = 2n_{eff}\Lambda \tag{2}$$

Therefore the Bragg wavelength (λ_B) of an FBG is a function of the effective refractive index of the fiber (η_{eff}) and the periodicity of the grating (Λ).

The photosensitivity phenomenon in optical fibers remained unexplored for several years after its discovery, mainly due the fact that the resulted Bragg wavelength was always a function of the wavelength of the light source used and very far away from the interested region of the spectrum, namely, the third telecommunication window. However, a renewed interest appeared years later with the demonstration of the side writing technique by Gerry Meltz and Bill Morey of United Technology Research Center [3] and later on with the possibility of tuning the Bragg wavelength into the C Band of the telecom spectrum.

Equation (2), also known as the Bragg reflection wavelength, is the peak wavelength of the narrowband spectral component reflected by the FBG. The FWHM (full-width-half-maximum) or bandwidth of this reflection depends on several parameters, particularly the grating length. Typically, the FWHM is 0.05 to 0.3 nm in most sensor applications. Figure 2 shows a typical Bragg reflection peak. The lateral lobes sometimes pose problems in automatic identification of the center wavelength and in telecom applications, such as wavelength division multiplexing (WDM), these side-lobes need to be suppressed in order to reduced the separation between the optical carriers, according to ITU-T-G.694.1 (International Telecommunications Union). The side-lobes can be suppressed during the FBG fabrication by a technique known as apodization.

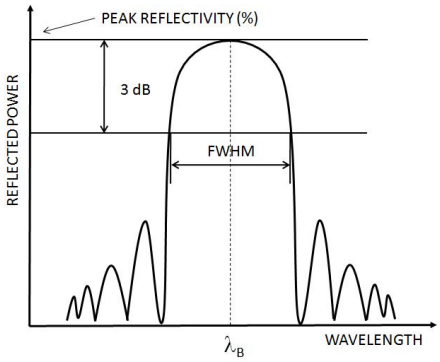

Figure 2. A typical Bragg reflection wave shape with its parameters defined.

From Eq. (2) we see that the Bragg wavelength only depends on the distance between gratings (Λ) and the effective index of refraction (n_{eff}).

Essentially, any external agent that is capable of changing Λ will displace the reflected spectrum centered at Bragg wavelength. A longitudinal deformation, due to an external force, for instance, may change both Λ and n_{eff}, the latter by the photo-elastic effect and the former by increasing the pitch of the grating. Equally, a variation in temperature can also change both parameters, via thermal dilation and thermo-optic effect respectively.

Therefore FBG is essentially a sensor of temperature and strain but, by designing the proper interface, many other measurements can be made to impose perturbation on the grating resulting in a shift in the Bragg wavelength which can then be used as a parameter transducer. Therefore, by using an FBG as a sensor we can obtain measurements of strain, temperature, pressure, vibration, displacement, etc.

Besides the influence of temperature and strain on the Bragg grating periodicity, one can also use n_{eff}, the fiber effective refractive index (RI) as a parameter transducer. The effective refractive index is an average of the RI of the core (n_{co}) and the RI of the cladding (n_{clad}) of the fiber. This parameter depends on how much the evanescent field of the core penetrates into the cladding. Since the fiber cladding diameter (125 μm) is much larger than the evanescent field, the effective RI is undisturbed by external influences. However by a corrosion of the fiber cladding by acid etching, one can reach the evanescent field which lies about 1.5 μm from the core interface. Now, the effective RI depends also on the surrounding RI, that is, the air, a gas or a liquid outside the fiber and we just created a device that can measure the RI of substances.

Since the strain or temperature measurements are encoded into wavelength shifts, these sensors are also self-calibrated because wavelength is an absolute parameter. Thus these sensors do not drift on the total light levels, losses in the connecting fibers and couplers or light source power. Additionally, the wavelength encoded nature of the output also allows the use of wavelength division multiplexing technique (WDM) by assigning each sensor to a different wavelength range of the available light source spectrum.

Using such a device and by injecting a spectrally broadband source of light into the fiber, a narrowband spectral component at the Bragg wavelength will be reflected by the grating. This spectral component will be missed in the transmitted signal, but the remainder of this light may be used to illuminate other FBGs in the same fiber, each one tuned to a different Bragg wavelength. The final result of such an arrangement is that we will have all Bragg peak reflections of each FBG back at the beginning of the fiber, each one in its specific wavelength range.

In order to calculate the sensitivity of the Bragg wavelength with temperature and strain we start from Eq. (2) and notice that the sensitivity with temperature is the partial derivative with respect of temperature:

$$\frac{\Delta\lambda_B}{\Delta T} = 2n_{eff}\frac{\partial\Lambda}{\partial T} + 2\Lambda\frac{\partial n_{eff}}{\partial T} \tag{3}$$

Substituting twice (2) in (3) we get:

$$\frac{\Delta\lambda_B}{\Delta T} = \frac{1}{\Lambda}\frac{\partial\Lambda}{\partial T}\lambda_B + \frac{1}{n_{eff}}\frac{\partial n_{eff}}{\partial T}\lambda_B$$

or rearranging,

$$\frac{\Delta\lambda_B}{\lambda_B} = \frac{1}{\Lambda}\frac{\partial\Lambda}{\partial T}\Delta T + \frac{1}{n_{eff}}\frac{\partial n_{eff}}{\partial T}\Delta T$$

The first term is the thermal expansion of silica (α) and the second term is the thermo-optic coefficient (η) representing the temperature dependence of the refractive index (dn/dT). Substituting we have:

$$\frac{\Delta\lambda_B}{\lambda_B} = (\alpha + \eta)\Delta T \tag{4}$$

The sensitivity with strain is the partial derivative of (2) with respect to displacement:

$$\frac{\Delta\lambda_B}{\Delta L} = 2n_{eff}\frac{\partial\Lambda}{\partial L} + 2\Lambda\frac{\partial n_{eff}}{\partial L} \tag{5}$$

Substituting twice (2) in (5), we have:

$$\frac{\Delta\lambda_B}{\lambda_B} = \frac{1}{\Lambda}\frac{\partial\Lambda}{\partial L}\Delta L + \frac{1}{n_{eff}}\frac{\partial n_{eff}}{\partial L}\Delta L \tag{6}$$

The first term in Eq. (6) is the strain of the grating period due to the extension of the fiber. Suppose we have a length L of a fiber with an inscribed FBG in it. If we apply a stress on the fiber of ΔL then we will have an relative strain $\Delta L/L$. At the same time if the FBG has a length L_{FBG} it will experience a strain $\Delta L_{FBG}/L_{FBG}$ but since the FBG is in the fiber, then $\Delta L_{FBG}/L_{FBG}=\Delta L/L$. Since the Bragg displacement with extension equals the displacement of the grating period with the same extension and, therefore, the first term in Eq. (6) is the unit.

The second term in Eq. (6) is the photo-elastic coefficient (ρ_e), the variation of the index of refraction with strain. In some solids, depending on the Poisson ratio of the material, this effect is negative, that is, when one expands a transparent medium, as an optical fiber for

instance, the index of refraction decreases due to the decrease of density of the material. Then, when an extension is applied to the fiber, the two terms in Eq. (6) produce opposite effects, one by increasing the distance between gratings and thus augmenting the Bragg wavelength and the other by decreasing the effective RI and thus decreasing the Bragg wavelength. The combined effect of both phenomena is the classical form of the Bragg wavelength displacement with strain:

$$\frac{\Delta\lambda_B}{\lambda_B} = (1 - \rho_e)\varepsilon_z \tag{7}$$

where ε_z is the longitudinal strain of the grating. Combining (4) and (7) together we finally end up with the sensitivity of the Bragg wavelength with temperature and strain:

$$\frac{\Delta\lambda_B}{\lambda_B} = (1 - \rho_e)\varepsilon_z + (\alpha + \eta)\Delta T \tag{8}$$

The parameters in (8) have the following values for a silica fiber with a germanium doped core:

$$\rho_e = 0.22,$$

$$\alpha = 0.55 \times 10\text{-}6/°C,$$

and

$$\eta = 8.6 \times 10\text{-}6/°C.$$

Thus the sensitivity of the grating to temperature and strain at the wavelength range of 1550 nm, after substituting the constants in (8) are:

$$\frac{\Delta\lambda_B}{\Delta T} = 14.18 \text{ pm}/°C \tag{9}$$

and:

$$\frac{\Delta\lambda_B}{\Delta\varepsilon} = 1.2 \text{ pm}/\mu\varepsilon \tag{10}$$

These theoretical values, though, are not absolute as each FBG of the same fabrication batch will present slightly different sensitivities, as we will see later in the following sections.

3. Temperature compensation

Equation (8) shows that the Bragg displacement is a function of both strain and temperature. By observing only $\Delta\lambda_B$ one cannot tell if the displacement was due to strain, temperature or both. If one wants to measure only temperature, the FBG must be protected against strain which can be simply done by loosely inserting the FBG into a small-bore rigid tubing. However, if one wants to measure strain, it is very difficult to stop variation of local temperature to reach the FBG; instead, we have to compensate this variation. In order to do this we have to measure the local temperature, by a thermistor, for instance, and apply Eq. (4) to calculate the effect of temperature alone in the Bragg wavelength displacement. Then,

the displacement of the Bragg wavelength due to strain alone is the total displacement observed minus the displacement due to temperature alone.

This approach is only valid if it was possible to electrically measure the temperature, which is not always the case since the local of interest could be a high voltage environment or a place with a high EMI.

The more elegant way is by the use of another FBG on the same fiber, protected against strain and at the same temperature as its neighbor. The two FBGs will be in the same fiber-optic and will provide two different Bragg reflections, one dependent on strain and temperature and the other dependent only on temperature, for compensation.

From Eq. (3) we have for the first FBG:

$$\Delta\lambda_{B1} = K_{\varepsilon 1}\Delta\varepsilon + K_{T1}\Delta T \tag{11}$$

Where

$$K_{\varepsilon 1} = (1 - \rho_e)\lambda_{B1} \tag{12}$$

$$K_{T1} = (\alpha + \eta)\lambda_{B1} \tag{13}$$

Similarly, for the other FBG we have:

$$\Delta\lambda_{B2} = K_{\varepsilon 2}\Delta\varepsilon + K_{T2}\Delta T \tag{14}$$

Where,

$$K_{\varepsilon 2} = (1 - \rho_e)\lambda_{B2} \tag{15}$$

$$K_{T2} = (\alpha + \eta)\lambda_{B2} \tag{16}$$

But since this FBG is strain free, the first term of (14) will not exist and $K_{\varepsilon 2}$ equals zero. Equations (11) and (14) can be written in matrix form:

$$\begin{bmatrix}\Delta\lambda_{B1}\\ \Delta\lambda_{B2}\end{bmatrix} = \begin{bmatrix}K_{\varepsilon 1} & K_{T1}\\ K_{\varepsilon 2} & K_{T2}\end{bmatrix} \times \begin{bmatrix}\Delta\varepsilon\\ \Delta T\end{bmatrix} \tag{17}$$

Equation (17) is called the wavelength shift matrix because its solution gives us the wavelength displacements of both FBGs as a function of temperature and strain. However, we need to find the sensing matrix that gives us the strain and temperature as a function of the wavelength displacement of each FBG. So, we multiply both sides of Eq. (17) by the inverse of the 2x2 matrix and get to:

$$\begin{bmatrix}\Delta\varepsilon\\ \Delta T\end{bmatrix} = \begin{bmatrix}K_{\varepsilon 1} & K_{T1}\\ K_{\varepsilon 2} & K_{T2}\end{bmatrix}^{-1} \times \begin{bmatrix}\Delta\lambda_{B1}\\ \Delta\lambda_{B2}\end{bmatrix} \tag{18}$$

Inverting the 2x2 matrix we have the sensing matrix:

$$\begin{bmatrix}\Delta\varepsilon\\ \Delta T\end{bmatrix} = \frac{1}{K_{\varepsilon 1}K_{T2} - K_{\varepsilon 2}K_{T1}} \begin{bmatrix}K_{T2} & -K_{T1}\\ -K_{\varepsilon 2} & K_{\varepsilon 1}\end{bmatrix} \times \begin{bmatrix}\Delta\lambda_{B1}\\ \Delta\lambda_{B2}\end{bmatrix} \tag{19}$$

In (19) we notice that if

$$K_{\varepsilon 1}K_{T2} \approx K_{\varepsilon 2}K_{T1} \tag{20}$$

then we would not have a possible solution for Eq. (19) because equations (11) and (14) would be two almost parallel lines. This would happen, for instance, if the two FBGs had the same coefficients and Bragg wavelength reflection and would, therefore displace equally. Notice that Eq. (12) and Eq. (15), as well as Eq. (13) and Eq. (16), respectively, differ only by the Bragg wavelength. So, to avoid the redundancy in Eq. (19) we can use FBGs with Bragg reflections wide apart.

Now we can solve Eq. (19) for strain and temperature:

$$\Delta\varepsilon = \frac{1}{K_{\varepsilon 1}K_{T2} - K_{\varepsilon 2}K_{T1}}\left(K_{T2}\Delta\lambda_{B1} - K_{T1}\Delta\lambda_{B2}\right) \tag{21}$$

$$\Delta T = \frac{1}{K_{\varepsilon 1}K_{T2} - K_{\varepsilon 2}K_{T1}}\left(K_{\varepsilon 1}\Delta\lambda_{B2} - K_{\varepsilon 2}\Delta\lambda_{B1}\right) \tag{22}$$

Equation (21) gives the real strain of FBG 1 as measured by $\Delta\lambda_{B1}$, compensated against temperature variation measured by $\Delta\lambda_{B2}$. Equation (22) gives the temperature of the sensors. It can be used for further compensation, as for instance the thermal dilation of the metallic parts of the setup.

4. Calibration of FBG with temperature and uncertainty assessment

As it will be seen below, Eq. (9) is not an exact model for the FBG behavior under temperature variation and therefore each FBG has to be independently calibrated in order to be possible to tell the temperature by the Bragg wavelength. In this section we demonstrate the procedure to calibrate an FBG chain made of five FBGs. In this study five FBGs were submitted to temperature variations between 20°C and 85°C in order to verify and quantify the parameters of Eq. (4) [4].

In order to measure temperature, we can use as many FBG as necessary, in different Bragg wavelengths; the only precaution is that each FBG's spectrum should not overlap with its neighbor during its displacement when the temperature varies. To obtain the largest range for five FBGs we distributed them along the available range of most FBGs interrogators, that is, 1530 nm-1570 nm.

The setup used to calibrate the FBGs is shown in Figure 3. The dotted square represents the optical system comprised of a commercial Bragg Meter (Spectral Eye 400 from FOS&S) that consists of an ASE (Amplified Spontaneous Emission) broadband source used to illuminate the FBGs via Port 1 of the optical circulator. The reflection spectrum of the FBGs returns through Port 2 and is directed via Port 3 to an embedded OSA where the reflected spectrum is detected and measured. All controls and data can be accessed by a computer connected to the USB port of the interrogator.

Figure 4 shows superimposed spectra of five FBGs recorded in a temperature variation from 20°C to 85°C.

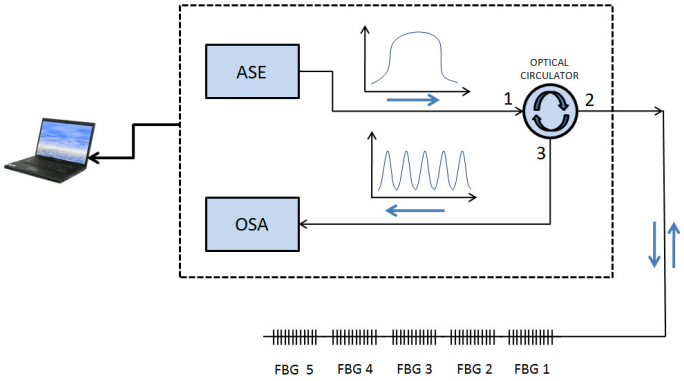

Figure 3. Schematic diagram of the measurement technique [4].

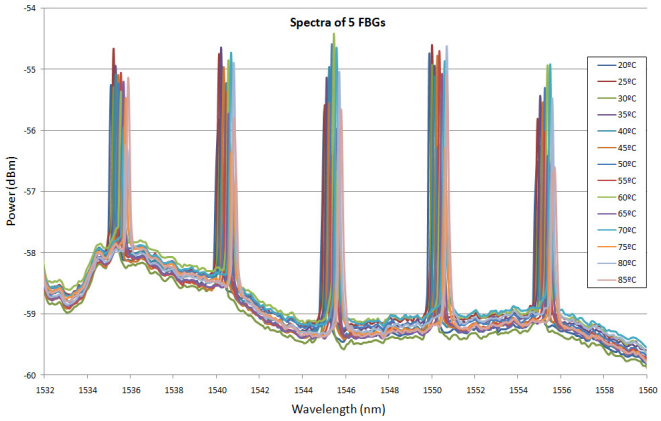

Figure 4. Superimposed spectra of five FBGs recorded in a temperature variation from 20ºC to 85ºC[4].

The procedure to calibrate the sensors followed the sequence: they were immersed simultaneously into a controlled temperature bath and the Bragg wavelengths were monitored and recorded along with the temperature given by a NIST-traceable thermometer (TD 990, Thermolink, 0.1°C resolution and ±1°C accuracy). Five sets of measurements were performed for each sensor in the range of 20°C to 85°C. Table I shows Bragg shift for each temperature and for each FBG.

From the data in Table 1 it is possible to calculate the sensitivity of each sensor, as predicted by (4) and the accuracy of the measurement chain. The graph in Figure 5 was built from the data in Table 1.

Table 2 shows a summary of the calibration parameters: the theoretical and experimental sensitivities, the correlation coefficients of the curve fittings, the root mean square errors (RMSE) and maximum residual errors.

T (°C)	Average Bragg wavelength peak (nm)				
	FBG1	FBG2	FBG3	FBG4	FBG5
25	1536,001	1540,928	1545,833	1550,819	1555,723
30	1536,067	1540,995	1545,903	1550,888	1555,793
35	1536,128	1541,059	1545,971	1550,959	1555,865
40	1536,183	1541,116	1546,03	1551,015	1555,922
45	1536,245	1541,177	1546,092	1551,083	1555,987
50	1536,310	1541,247	1546,163	1551,147	1556,055
55	1536,368	1541,308	1546,224	1551,213	1556,119
60	1536,427	1541,368	1546,284	1551,273	1556,178
65	1536,497	1541,440	1546,358	1551,345	1556,253
70	1536,557	1541,501	1546,420	1551,408	1556,317
75	1536,618	1541,566	1546,484	1551,469	1556,383
80	1536,680	1541,627	1546,549	1551,539	1556,447

Table 1. Average Bragg center wavelength of each FBG under temperature variation [4]

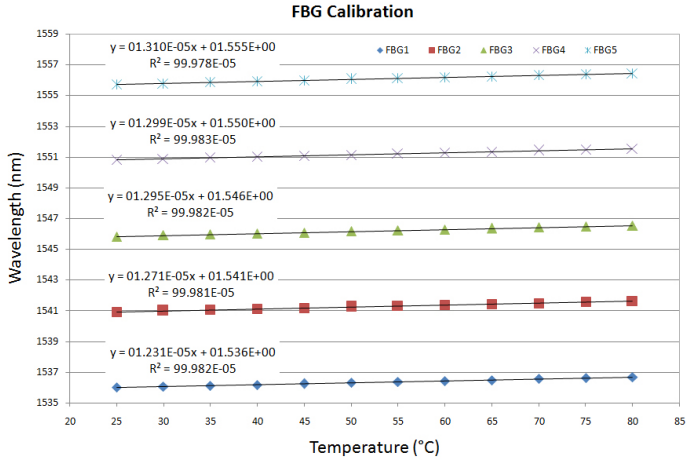

Figure 5. Wavelength shift versus temperature for each FBG [4].

FBG #	Theoretical Sensitivity (pm/°C)	Measured Sensitivity (pm/°C)	Correlation Coefficient (R^2)	RMSE (°C)	Max. Residual Error (°C)
1	14.05	12.31	0.99982	0.00311	0.003
2	14.10	12.71	0.99981	0.00328	0.005
3	14.14	12.95	0.99982	0.00327	0.005
4	14.19	12.99	0.99993	0.00320	0.006
5	14.23	13.10	0.99978	0.00363	0.007

Table 2. Calibration Parameters [4]

Figure 6 shows the error analysis for FBG1; the maximum positive error was approximately 0.004°C at 30°C. The temperature error measurements for other sensors were within the range of ±0.007°C.

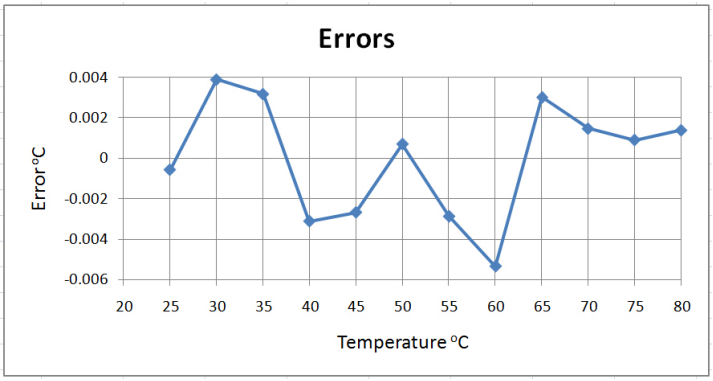

Figure 6. Error analysis for FBG 1 [4].

All correlation coefficients are very close to unity and errors much smaller than 1°C. These errors are a combination of the uncertainty of the interrogation system, (±1 pm) and of the thermometer used. Using the FBG's average sensitivity of 13 pm/°C (see Table 2), 1 pm in error means a temperature uncertainty of about 0.08°C which is much smaller that the error produced by the thermometer.

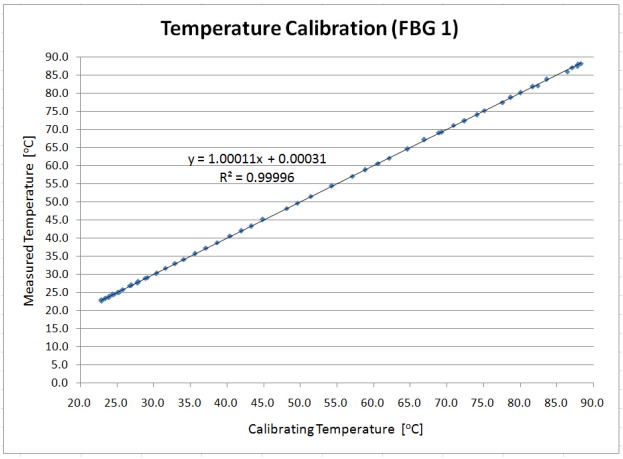

Figure 7. Temperature calibration responses of FBG 1 [4].

Notice in Table 2 that the theoretical sensitivities predicted by Equation (3) are different from those obtained in the calibration experiment. Also, Eq. (1) shows λ_B as a function of n_{eff}, the average index of refraction between the pristine fiber core and that of the Ultra-Violet (UV)-irradiated core. The FBG fabrication processes is not automatic and the radiation time

for each FBG inscription is not the same as the laser is turned off by the operator when Bragg reflection appears above the desired level. The UV modifies the index of refraction of the fiber core and also modifies the values of η in each FBG differently. These results in the slightly dispersed sensitivities found above. This effect is confirmed by [5] that demonstrated a technique for changing the temperature responsivity of FBGs through increased UV exposure over the FBG.

From the data in Table 2 it is possible to calculate the relationship between wavelength and temperature for each FBG. to-one fitting accuracy to the third decimal place in temperature and a correlation coefficient R^2=0.99996, demonstrating a very good linearity and accuracy of FBG sensors for temperature measurements.

5. Photosensitivity in optical fibers

Photosensitivity in glass, as mentioned in Session 2, was discovered at the Communications Research Center in Canada, in 1978 by Hill and co-workers [1]. It was a new nonlinear effect in optical fibers and was called at that time of fiber photosensitivity.

A decade later after this discovery, Meltz and co-workers [3] have proposed a model for fiber photosensitivity. What motivated their model was that at first, fiber photosensitivity was detected only in fibers containing germanium as a dopant.

The model is based on the fact that when germanium-doped silica fibers are fabricated by MCVD technique, germania (GeO_2) and silica (SiO_2) in form of gases combine in high temperatures to produce the fiber. During the process though, there is a statistical probability that products like Ge-Ge, O-Ge-O, Ge_2^0 and Ge-Si might be formed, which are defects in the fiber lattice and are called in the literature as “wrong bonds”. The fiber presents strong absorption peak at 245 nm, which is associated with these defects. When these defects are irradiated with UV light some absorptions bands appear and the index of refraction increases in these points.

The origins of photosensitivity and the change of the RI as a consequence have yet to be fully understood as no single model can explain the experimental results shown in the literature. So, it becomes apparent that photosensitivity is a function of several mechanisms such as photochemical, photomechanical, thermochemical, etc. [6].

One of the models that show consistencies with experimental results seems to be the compaction model based on the Lorentz-Lorenz law which states that the RI increases with material compression. This idea was pursued

These equations were fed into the software of the FBG interrogation system which returns the temperature of each sensor in a field application. Finally, it is possible to plot the calibrating temperature against measured temperature, as shown in Figure 7, presenting a one-by [7] that used UV Laser irradiation to produce thermally reversible, linear compaction in amorphous SiO_2. An accumulated, incident dose of 2000 J/cm^2 would produce an irreversible compaction and photoetching. The above results are in accordance with the

fabrication of Type I and Type IIA FBG. Also, Laser compaction results were found to be consistent with those obtained using hydrostatic pressure. Therefore it was observed an approximately linear RI versus ΔV/V agreeing with the predictions of the Lorentz-Lorenz law.

Also, in accordance with this model of densification associated with the writing of Bragg gratings, Riant and co-workers [8] observed a transition mechanism between Type I and Type II gratings.

Notice that, when a transparent material is compressed we observe two effects that interfere with the RI. One is the increase of RI due to the increase of density of the material. The other is the photoelastic effect, which is negative for many optical media, and produces an opposite effect. However the compression produces an effect much stronger than the photoelastic effect and we normally observe an increase of RI in the irradiated parts of the FBG.

With the knowledge that the UV irradiation produces an increase on the RI we can now go further and observe physically the FBG. Figure 8 shows the core's RI along the length of the fiber (z axis) with most frequent values of the parameters. The effective RI of the core is the average index of refraction of the irradiated portion of the core and is approximately 1.45. Due to the UV radiation the variation of the RI is about $\Delta n=10^{-4}$. The grating period (Λ) is the same as the interference pattern, about 500 nm and the FBG length L_{FBG} is around 10 mm.

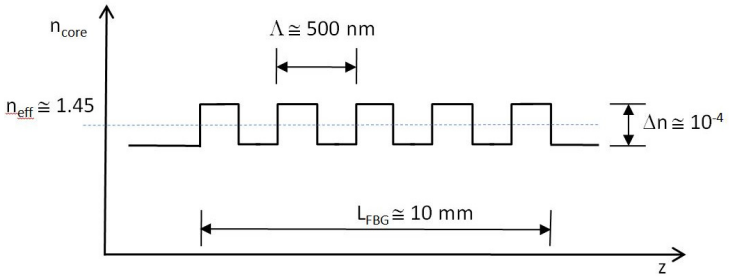

Figure 8. The Refraction Index variation of the fiber core along the length of the fiber (z axis) with most frequent values of the parameters.

The interference pattern, however, does not vary as a square wave but rather as an approximate sinusoidal waveform, which will inscribe an RI variation on the fiber of the same form, as shown in Fig. 9. In the figure, n_{eff} is the RI of the pristine fiber core, $\langle n_{eff} \rangle$ is the average RI in the FBG region, Δn_{DC} is the average amount of RI increased by the UV dose and Δn_{AC} is half of the total RI variation in the FBG.

The mathematical model of the RI in the FBG area as a function of the UV radiation dose (d) in Joules and the distance z along the fiber's axis is [9]:

$$n_{eff}(z,d) = n_{eff} + \left(\Delta n_{DC}(d) + \Delta n_{AC}(d)\sin\frac{2\pi}{\Lambda}z\right) \quad (23)$$

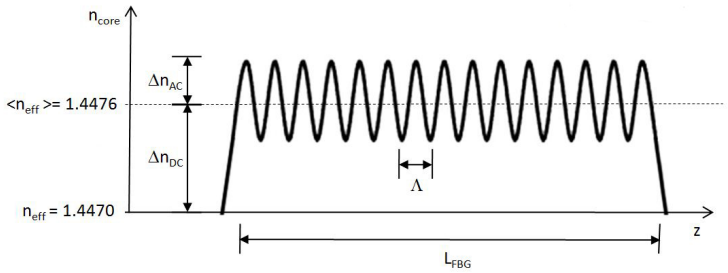

Figure 9. Variation of the Refraction Index of the fiber`s core along the length of the fiber (z axis) resultant of a sinusoidal diffraction pattern [9].

Notice that both Δn_{DC} and Δn_{AC} increase with UV dose and, since the UV radiation is never zero along the diffraction region, all FBG length experiences an increase of RI.

Now we can rewrite Eq. (2) using the average RI in the FBG area:

$$\lambda_B = 2\langle n_{eff}\rangle\Lambda \tag{24}$$

For an FBG inscription using the setup of Figure 11, it is necessary first to calculate the angle φ for the desired Bragg wavelength. Then, the operator monitors the reflection spectrum until the reflectivity reaches the desired value. But since $\langle n_{eff}\rangle$ increases during the irradiation, so does λ_B, according to Eq. (24). Figure 10 shows the progression of an FBG reflection spectrum as UV dose increases.

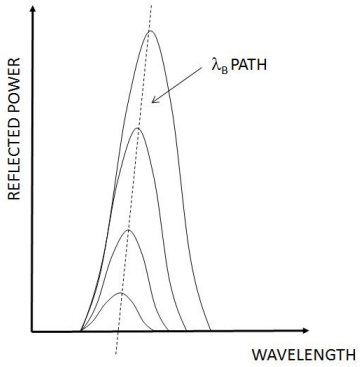

Figure 10. Progression of an FBG reflection spectrum as UV dose increases [9].

The dotted line in Figure 10 shows the path of the Bragg wavelength as UV dose increases, or same to say, the variation of $\langle n_{eff}\rangle$, according to Eq. (24).

Therefore, two relationships can be obtained from Figure 10:

$$\text{Reflectivity} = f(\text{number of shots or irradiation time}) \tag{25}$$

$$\lambda B = g(\text{number of shots or irradiation time}), \tag{26}$$

where f(*) And g(*) are arbitrary functions to be determined by curve fitting.

Both reflectivity and Bragg wavelength increase with the number of laser shots because each shot represents a certain amount of UV energy and the energy is integrated producing the stress inside the fiber core. These equations will be important when an FBG is designed.

As UV dose increases, so does reflectivity, but up to a threshold above which the reflectivity starts do lower again. This is due to the competing effects between the increase of RI due to the increase of density of the material and the photoelastic effect, which is negative for many optical media. Above the threshold limit, the photoelastic effect is stronger than the increase of density, probably because this last effect saturates while the photoelastic effect does not. The threshold is about 500 mJ/cm^2 and this value is considered to be the limit separating Type I gratings to Type IIA. While during the formation of Type I FBG, λ_B experiences a red shift (see Figure 10), during the erasure of the FBG in type IIA formation, the Bragg wavelength experiences a blue-shift. Above this limit, the FBG starts to be erased until it completely disappears.

Bragg grating in germanosilacate fibers exhibits a temperature decay dependency. Type I FBGs are found to present reasonable short term stability up to 300°C, whereas Type IIA gratings exhibit very good stability up to 500°C [6].

Therefore, after fabricating a Type I FBG it is recommended to submit them to an annealing process up to a temperature that exceeds the service temperatures of the application in order to produce an accelerated ageing.

Conventional telecommunication fibers normally present around 3.5% concentration of germania doping. These fibers will weakly respond to UV radiation ($\Delta n \cong 10^{-5}$) and will grow low reflectivity FBGs. Only fiber with 5% plus GeO concentration present photosensitivity enough to be useful for FBG fabrication, but are more expensive than conventional telecommunication fibers. Those fibers with up to 30% of dopant concentration are produced by several fiber makers such as Nufern, Fibercore and IPTH.

Another dopant used is GeO co-doped with boron; these fibers present an enhanced sensitivity however causing an increase in losses. Therefore, boron co-doped fibers are not good for long sensing distance, they are limited to some few meters only in contrast with pure GeO doped fibers that can be used to remotely monitor parameters which are several kilometers away from the interrogation system.

Another way of enhancing the fiber sensitivity is by hydrogen diffusion into the fiber core. The mechanism causing an increased sensitivity is thought to be due the reaction of H_2 with GeO. In highly doped fibers there is a significant concentration of Ge-O-Ge bonds. H_2 reacts with these bonds resulting in the formation of Ge-OH, which absorbs UV radiation and therefore increasing the internal stress into the core of the fiber [10].

The hydrogen diffusion is accomplished by leaving the fiber into a tight enclosure with hydrogen at high pressure. Pressures from 20 atm to 750 atm can be used but most commonly 150 atm. Apart from increasing the fiber photosensitivity, hydrogen loading allows the fabrication of FBG in any germane silicate and germanium free fibers.

When a hydrogen loaded fiber is taken out of the high pressure vessel it is as soft as cotton string. However, by heating the fiber after the exposition, the hydrogen diffuses out in a few minutes.

Hydrogen loading can be also accomplished by a technique known as flame brushing. This technique consists in burning for 20 minutes the fiber by a hydrogen-oxygen flame reaching temperatures of 1700ºC. At high temperature, the excess of hydrogen in the mixture diffuses into the fiber. The advantage of frame brushing is that it is possible to sensitize conventional telecommunications fibers. The disadvantage, however, is that the flame burns the fiber acrylate buffer in an area larger than that of the FBG itself which demands a posterior fiber recoating.

6. Fabrications techniques

As mentioned above the interest in FBG started with the possibility of inscribing the grating sideways as demonstrated by Meltz [3] and with the possibility of tuning to a desired wavelength along the telecom band. From then on, many FBG applications appeared first in telecom such as add/drop, dense wavelength division multiplexing (DWDM) mux/demux, filters, lasers, and so on. Later, with the telecommunications devices and equipments decreasing prices, FGBs started to be used as sensors in a commercial basis.

The first technique used to inscribe a FBG in the fiber was the interferometer and it is used in many different configurations (Figure 11 shows a basic interferometer). A laser beam is divided in two by a beam splitter or a prism. Each part is reflected in mirrors to meet again to form a interference pattern over the fiber to be inscribed. Cylindrical lenses concentrate the beams in the inscribing area of the fiber, about 5 mm by 200 μm in order to increase the density of the UV dose.

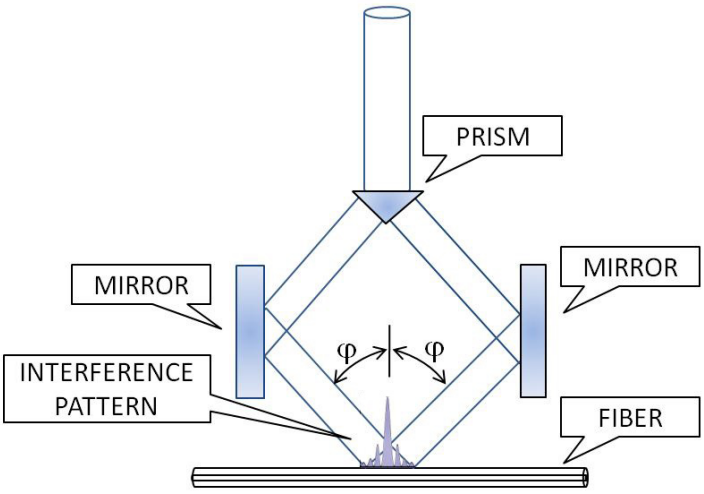

Figure 11. A basic interferometer.

The period of the interference pattern (Λ) depends on the wavelength of the light used for writing (λ_{Laser}) and also on the half-angle between the two interfering beams (φ) as shown in Eq. (27).

$$\Lambda = \frac{\lambda_{Laser}}{2\sin\varphi} \tag{27}$$

There are some disadvantages when using such arrangement as, for instance, the difficult to align the beams, the necessity to achieve a very good spatial coherence on the laser and problems associated with air flow which slightly modifies the RI of the air distorting the wave front of the beams. This effect could lead to an FBG of poor quality. The advantage is that one can adjust the mirrors in order to vary the grating period to virtually any value around the telecommunication band.

Nowadays we rely on the phase-mask technique which is a diffractive optical element that spatially modulates the UV beam with period Λ_{pm}. The phase masks are formed in a fused silica substrate by a holographic technique or electron beam lithography.

When a laser beam is incident to the phase mask a diffraction occurs and the beam is divided into several diffraction orders. The zero order is suppressed to less than 3%, but the +1 and -1 orders prevail with most of the remaining power. These two orders start from the same point on the other side of the phase mask but are divergent. At the near field an interference pattern is produced as the two orders cross each other, with a period

$$\Lambda = \frac{\Lambda_{pm}}{2} \tag{28}$$

The optical fiber is placed in contact or in close proximity to the phase mask, inside the near field where the interference pattern is produced as shown in Figure 12. An increased power density can be achieved by the use of a cylindrical lens parallel to the fiber, before the phase mask.

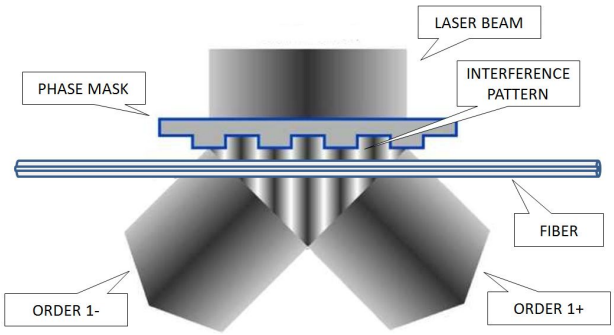

Figure 12. A laser beam inscribing gratings in a optical fiber through a phase mask.

The advantage of the phase mask is that its setup is much simpler because there is no need for the laser to have a good coherence and there are no mirrors to align. However, as the phase mask is such a fragile optical element, the close proximity of the fiber to the phase

mask surface can scratch it. If the distance between the phase mask is increased by a few millimeters the fiber will be illuminated by a narrower interference and the FBG will be accordingly narrower. Another disadvantage of the phase mask technique is that the periodicity of the FBG inscribed is fixed by the one of the phase masks, according to Equation (28).

An alternative setup is shown in Figure 13 in which the phase mask is far away from the fiber and the two mirrors redirect the +1 and -1 refracted orders back to the fiber.

The advantage of such setup is that one can adjust the Bragg wavelength by the angles of the mirrors.

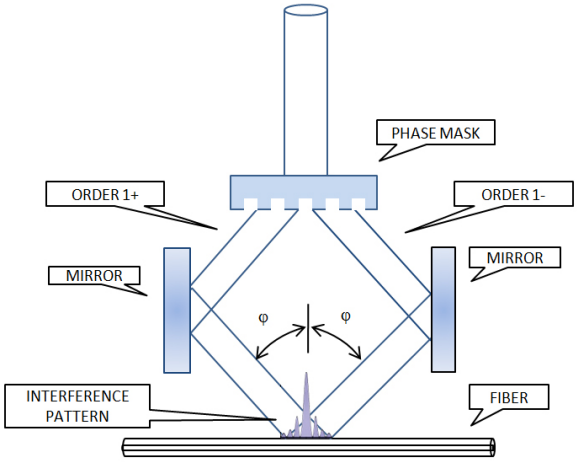

Figure 13. Most common setup used with a phase mask.

7. FBG fabrication parameters

When specifying an FBG the following parameters must be known:

- Central Brag wavelength, λ_B
- FBG width, FWHM
- Reflectivity

Bragg wavelength(λ_B) depends essentially on the phase mask periodicity or on the laser wavelength, and on the intersection half-angle in the case when an interferometer setup is used (Figure 11). However, the UV dose also modifies the Bragg wavelength, according to Eq. (25).

FWHM depends on the FBG length and on the UV dose, according to the following Equation [6]:

$$\mathrm{FWHM} = \lambda_B S \sqrt{\left(\frac{\Delta n}{2n_{eff}}\right)^2 + \frac{1}{N}^2} \tag{29}$$

where, Δn is the amplitude of the induced RI in the fiber, $\Delta n = 2 \times \Delta n_{AC}$ (see Figure 9), λ_B is the final Bragg wavelength, s is 1 for strong reflection grating with reflectivity close to 100%, or 0.5 for weak gratings, N is the number of grating planes, $N = L_{FBG}/\Lambda$.

Reflectivity, as it has been seen in later sessions, is a function of the UV dose in J/m^2, the amount of Germania doping in the fiber and the hydrogenation processes. Equation (26) can be useful for predicting the reflectivity and this parameter can also be adjusted by varying the FBG length. This is accomplished by adjusting the laser beam width. One can produce lengths as small as 2.5 mm obtaining, thus very low reflectivity and lengths as large as 15 mm obtaining a reflectivity around 100%.

Therefore, when projecting an FBG inscription, one has to carry out an inverse engineering to preview how much λ_B will displace during the inscription to the desired reflectivity and decrease this value to the desired Bragg wavelength in order to adjust the mirrors accordingly.

As none of the above parameters are not precisely known, the best way to know the exact time of irradiation is by experimental tests.

8. Interrogation techniques for FBG sensors

The main challenge when it comes to FBG sensing is the method to demodulate its wavelength changes. The use of FBG sensors is connected to the development of techniques to interrogate these sensors and detect Bragg wavelengths shifts as a function of the parameter being measured.

The easiest way to interrogate an FBG is by the use of an optical spectrum analyzer (OSA) which performs a direct measurement of the reflection spectrum of the FBG. The other method is based on the conversion of wavelength variations into optical power intensities.

The technique using an optical spectrometer is very simple. The interrogation system consists of a broadband optical source which illuminates the FBGs. Their reflected peaks, which are represented by each Bragg wavelength λ_B, are directed to the OSA and monitored by a computer, as shown in Figure 3.

Although being a simple demodulation technique, it presents some disadvantages: first, the commercial OSAs are heavy and expensive equipment, besides being inappropriate for field applications. Moreover, most of the spectrum analyzers are limited to static measurements, so they don't have sufficient resolution concerning the response time when a number sensors are being interrogated. A conventional OSA will present an accuracy of about ±50 pm, which would produce errors of about ±4°C and ±60 με, according to equations (9) and (10). For most applications these errors are unacceptable if compared to conventional resistive temperature detectors (RTD) and strain gauges. To detect small variations in wavelength the development of new techniques must also ensure essential characteristics such as static and dynamic measurements, real-time measurements, accuracy, resolution, and low cost, all necessary conditions for field applications. In conclusion this technique is only useful for laboratory applications and tests.

The setup shown in Figure 3 is also commercially available by a few companies as standalone equipment and appropriated to go to the field. In this case they feature resolutions as good as ±2 pm and can be programmed to monitor specific parameters as pressure, strain, temperature, etc. However, due to the high cost, they will be applicable to solve monitoring needs of industries only if the project included as many sensors as possible to be monitored by one single unit to have the total price divided by the number of sensors.

The other demodulation technique uses a Fabry-Perot (FP) tunable filter. Although the interferometric FP filter method is a consolidated technology, showing high resolution and accuracy, it still presents a moderate cost. The tunable optical filter scheme is based on a Fabry-Perot extrinsic cavity, which is adjusted by mirrors and by varying the internal cavity of a PZT crystal by means of an external power supply, enabling the filter adjustment and selection of the desired wavelength. This relationship between the changes in the filter wavelength as a function of an applied voltage is linear. Defects in the geometry of the lens during the filter manufacturing process can cause instability in the measurement system, so that the optical spectrum of the filter is not entirely symmetrical.

The demodulation setup using a FP filter is shown in Figure 14. A broadband light source was used to illuminate the FBG sensor via an optical circulator. The reflected spectrum of the sensor passes through the FP tunable filter with a 0.89 nm bandwidth.

This demodulation technique is based on the same principle of an FM radio signal demodulated by an edge filter. The signal waveband is made to vary at the wedge of a filter that will transmit a variable power proportional to the variation of the signal frequency. In our case, proportional to Bragg shift. In reality, the transmitted signal through the filter is proportional to the convolution between the signal power and the filter response.

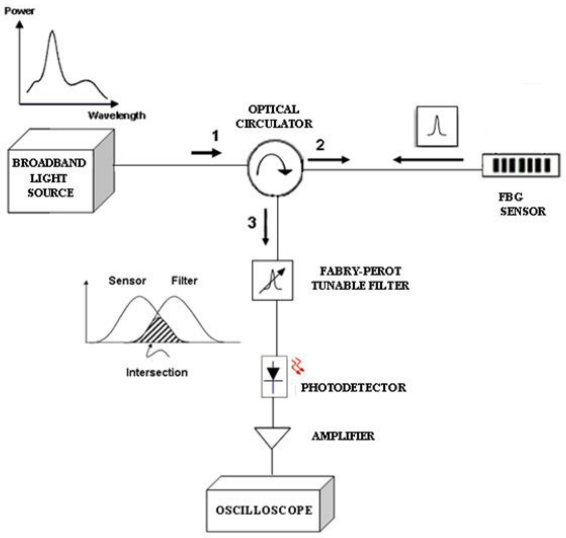

Figure 14. The interrogation setup using a Fabry-Perot filter (adapted from [11]).

The optimum position of the center wavelength of the FP filter is chosen by an algorithm described by [11]. The dashed area on the spectra drawing (inset in Figure 14) is the intersection between the spectrum of the reflected signal and the band pass of the FP filter. The integral of this area represents the total light power that reaches the photodetector.

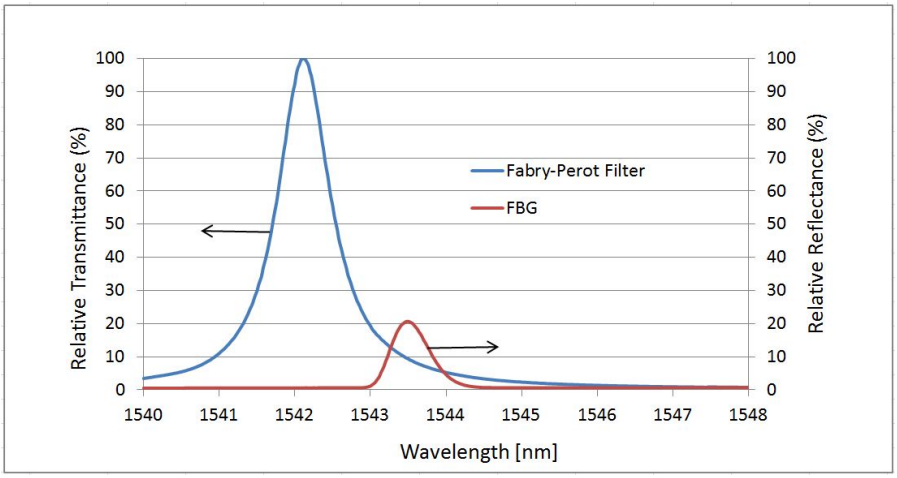

Figure 15. Spectral curves for the Fabry-Perot filter, $F_{FP}(\lambda)$, and the FBG, $F_{FBG}(\lambda)$.

The spectral curves for the FP filter, FFP(λ), and for the FBG, $F_{FBG}(\lambda)$, are shown in Figure 15, where the sensor is at quiescent state. The vertical axes show the relative transmittance of the FP filter and the relative reflectance of the FBG sensor, respectively. The numerical convolution $F_{FP}(\lambda)*F_{FBG}(\lambda)$ represents the available power to the photodetector as a function of the wavelength shift. The convolution curve is shown in Figure 16.

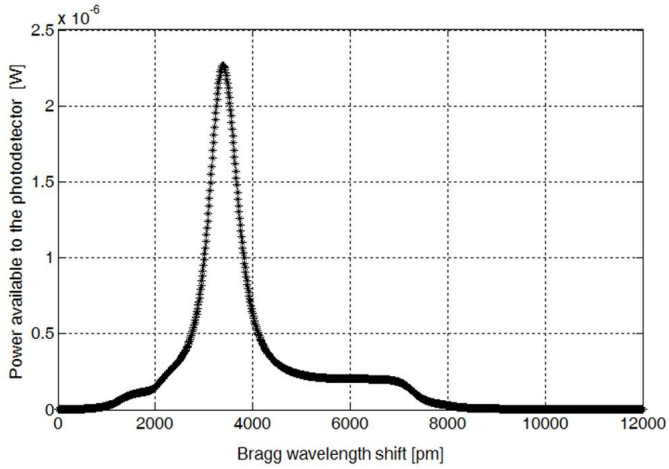

Figure 16. The convolution between $F_{FP}(\lambda)*F_{FBG}(\lambda)$.

Instead of an FB filter, it is possible to use another FBG, in this case used as a dichroic mirror, differently from the FP filter which acts by light transmission. A broadband light source injects light into port 1 of the optical circulator 1. The light circulates to port 2, illuminating the FBG sensor. The reflection spectrum of the FBG sensor is deviated to port 3, and enters through port 1 of circulator 2. Circulator 2 deviates the signal to the twin FBG filter, through port 2. Only the superimposed wavelengths (inset graphic) reflect back to circulator 2, which deviates the light to the photodetector through port 3.

This demodulation scheme is very simple, and reduces the cost of the setup implementation; however, the twin FBG must be manufactured at an exact wavelength to provide an optimized operation procedure.

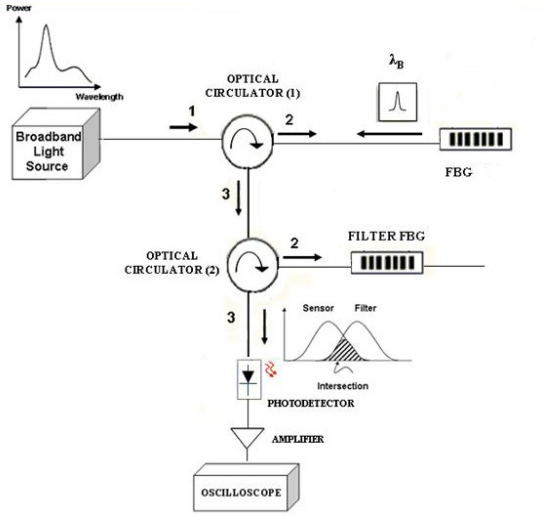

Figure 17. Schematic diagram of experiment for AC voltage measurement by using the twin grating filter technique [11].

Author details

Marcelo M. Werneck, Regina C. S. B. Allil, Bessie A. Ribeiro and Fábio V. B. de Nazaré
Instrumentation and Photonics Laboratory, Electrical Engineering Program, Universidade Federal do Rio de Janeiro (UFRJ), RJ, Brazil

Regina C. S. B. Allil
Division of Chemical, Biological and Nuclear Defense, Biological Defense Laboratory, Brazilian Army Technological Center (CTEx) RJ, Brazil

9. References

[1] Hill, K.O.; Fujii, Y.; Johnson, D. C.; Kawasaki, B. S., "Photosensitivity in optical fiber waveguides: application to reflection fiber fabrication", Appl. Phys. Lett. 32 (10): 647, 1978.

[2] Hill, K.O., "Photosensitivity in Optical Fiber Waveguides: From Discovery to Commercialization" IEEE Journal on Selected Topics in Quantum Electronics, VOL. 6, NO. 6, pp. 1186-1189, November/December 2000

[3] Meltz, G., Morey, W. W. and Glenn, W. H., "Formation of Bragg gratings in optical fibers by a transverse holographic method", Opt. Lett. 14 (15): 823, 1989.

[4] Werneck, M. M., Allil, R. C. and Ribeiro, B. A., "Calibration and Operation of a Fiber Bragg Grating Temperature Sensing System in a Grid-Connected Hydrogenerator", IET Science, Measurement & Technology, accepted to publication on September, 2012.

[5] Gwandu, B. A. L. and W. Zhang, W., "Tailoring the temperature responsivity of fibre Bragg gratings", Proceedings of IEEESensors, DOI: 10.1109/ICSENS.2004.1426454, pp. 1430-1433, Volume 3, 2004.

[6] Othonos, A., Kalli, K., "Fiber Bragg Gratings – Fundamentals and Applications in Telecommunications and Sensing", Artech House, 1999.

[7] Fioria, C., and Devinea, R. A. B., "Ultraviolet Irradiation Induced Compaction and Photoetching in Amorphous Thermal SiO2". MRS Proceedings of the Fall Meeting, Volume 61, 1985.

[8] Riant, I., Borne, S., Sansonetti, P., Poumellec, B. "Evidence of densification in UV-written Bragg gratings in fibres", in Photosensitivity and Quadratic Nonlinearity in Glass Waveguides: Fundamentals and Applications, pp: 52-55, Postconference Edition, Optical Society of America, 1995.

[9] Jülich, F. and Roths, J., "Determination of the Effective Refractive Index of Various Single Mode Fibres for Fibre Bragg", Proceedings of SENSOR+TEST Conference (OPTO-2009), Nürnberg, pp 119-124, 2009.

[10] Lemaire, P. J., Hill, M. and Erdogan, T., "Hydrogen-enhanced UV photosensitivity of optical fibers: Mechanisms and reliability", in Photosensitivity and Quadratic Nonlinearity in Glass Waveguides Fundamentals and Applications, September 9-11, 1995, Portland, Oregon, Technical Digest Series, Volume 22, pp 78-81.

[11] Ribeiro, B. A., Werneck, M. M. and Silva-Neto, J. L., "A Novel Optimization Algorithm to Demolutate a PZT-FBG sensor in AC High Voltage Measurements", in review at IEEE Sensors Journal, September, 2012.